Bioprocess Biosyst Eng (2011) 34:931–938
DOI 10.1007/s00449-011-0544-9

ORIGINAL PAPER

Direct electron transfer and electrochemical study of hemoglobin immobilized in ZnO hollow spheres

Changhua Liu · Jing Xu · Zongfang Wu

Received: 6 December 2010 / Accepted: 5 April 2011 / Published online: 20 April 2011
© Springer-Verlag 2011

Abstract ZnO hollow spheres were firstly prepared. A new type of amperometric hydrogen peroxide biosensor was fabricated by entrapping Hemoglobin (Hb) through the ZnO hollow spheres (ZHS) nanoparticles. The composition morphology and size were studied by transmission electron microscopy. The surface topography of the prepared films was imaged by atomic force microscope (AFM). Several techniques, including UV–vis absorption spectroscopy, cyclic voltammetry, chronoamperometry were employed to characterize the performance of the biosensor. The results indicated that the ZHS nanoparticles had enhanced the performance of the hydrogen peroxide sensors. The electrochemical parameters of Hb in the ZHS were calculated by the results of the electron-transfer coefficient (α) and the apparent heterogeneous electron-transfer rate constant K_s as 0.5 and 3.1 s^{-1}, respectively. The resulting biosensors showed a wide linear range from 2.1×10^{-6} to 5.18×10^{-3} M, with a low detection limit of 7.0×10^{-7} M (S/N = 3) under optimized experimental conditions. The results demonstrated that the ZHS matrix may improve the protein loading with the retention of bioactivity and greatly promote the direct electron transfer, which can be attributed to its unique morphology, high specific surface area, and biocompatibility. The biosensor obtained from this study possesses high sensitivity, good reproducibility, and long-term stability.

C. Liu (✉) · J. Xu · Z. Wu
Key Laboratory on Luminescence and Real-Time Analysis, Ministry of Education, College of Chemistry and Chemical Engineering, Southwest University, Chongqing 400700, People's Republic of China
e-mail: chliu@swu.edu.cn

Keywords Biosensor · Direct electron transfer · ZnO hollow spheres · Hemoglobin

Introduction

There has been increasing interest in studying redox proteins/enzymes in order to achieve direct electron transfer for applications in mediator-free biosensors, bioreactors and biomedical devices [1–3]. However, as their redox centers are usually deeply buried within the protein molecules, it is difficult for electron to direct transfer between proteins and electrode. Hence, various materials are exploited to immobilize redox proteins on electrode surface [4]. Generally, those materials are nontoxic, stable and biocompatible, such as surfactants [5], polymers [6], nanomaterials [7], and inorganic mesoporous materials [8] and so on. In order to attain native structure and appropriate orientation of the enzyme, appropriate materials were applied to modify the electrode. So the improvement of electron transfer between the enzyme and the electrode has been very popular in recent years [9–11].

Hollow spheres represent a fascinating class of materials, which has attracted an immense interest of the researchers because of their potential applications in bioanalytical area catalysis, magnetics, ceramics, pigments and biosensor [12–15]. Research has demonstrated a clear ZnO size and shape dependence of its electromagnetic, optical, and catalytic properties [16]. For example, ZnO sol–gels possess high surface area, good biocompatibility, chemical and photochemical stability [17]; ZnO microspheres may provide a desirable microenvironment for the enzymes to retain their enzymatic stability and activity by limiting the conformational change and unfolding of the entrapped enzymes [18]. This has motivated our motivity

in research on ZnO shape dependence of its electronic properties applied to electrocatalysis and biosensor.

In this work, ZnO hollow spheres (ZHS) were firstly prepared, and then Hemoglobin (Hb) and biocompatible composite ZHSs were successfully electro-codeposited onto the surface of gold electrode. The direct electron transfer of Hb was promoted greatly, and a pair of well-defined and quasi-reversible redox peaks occurred. The direct electrochemistry and analytical performance of the resulting biosensor were investigated. And the immobilized Hb retained its natural structure and showed high electrocatalytic activity to the reduction of H_2O_2.

Experimental

Reagent and materials

Hemoglobin (bovine blood) was obtained from Sigma. China. 0.1 M phosphate buffered saline (PBS) containing 0.1 M KCl with various pH values were prepared by mixing the stock solutions of K_2HPO_4 and KH_2PO_4, and adjusted by 0.1 KOH and 0.1 M H_3PO_4 solution. Hydrogen peroxide (30% w/v solution) was purchased from Chemical Reagent Company, Chongqing, China and the concentration of the more diluted hydrogen peroxide solutions prepared from 30% hydrogen peroxide was determined by titration with potassium permanganate. Poly(vinylpyrrolidone) (PVP, MW = 30,000), 2,2-azobisisobutyronitrile (AIBN), absolute ethanol, sulfuric acid (H_2SO_4, 98%), sodium hydroxide (NaOH), aqueous ammonia solution (28 wt%), zinc acetate dihydrate ($Zn(Ac)_2{\cdot}2H_2O$), and styrene (St) were purchased from Chongqing Chemical Reagent Co. (China). All other reagents were of analytical reagent grade and used as received. Doubly distilled water was used in this experiment throughout.

Instrumentation

Electrochemical measurements were carried out on CHI 660A electrochemical workstation (CH Instruments, Chenhua Co., Shanghai, China). UV–vis absorbance spectroscopy was performed using a UV-2205 spectrophotometer (Shimadzu, Kyoto, Japan). The morphology of ZHS was investigated by transmission electron microscopy (TEM, JEM-100CXII, Japan). Atomic force microscope images were obtained with scanning microscope probe (AFM, Vecco, USA).

Preparation of ZnO hollow spheres

ZnO hollow sphere was prepared according to the following procedure. ZHS was synthesized using the sulfonated polystyrene (PS) core–shell spheres as the template spheres. The method of synthesis of the sulfonated PS spheres was described elsewhere [19]. $Zn(Ac)_2{\cdot}2H_2O$ was dissolved in absolute ethanol, the sulfonated PS spheres ethanol solution was added dropwise to it under magnetic stirring. The mixed solution was stirred at 60 °C for 1 h, and then ethanol solution containing NaOH was dropped into the mixture and stirred at 60 °C for another 2 h. The solution was then filtered and the cake was washed with ethanol and water. ZHSs were obtained after the cake was heated in air at 500 °C for 2 h to remove the PS templates [19–21].

Preparation of the enzyme electrodes

A bulk gold disk electrode ($\phi = 4$ mm) was polished to a mirror-like surface with 0.3, 0.05 μm alumina slurry on microcloth pads, and sonicated in ethanol and distilled water. Then gold electrode was chemically cleaned by repeated potential scanning in 0.5 M H_2SO_4 solution in the potential range of −0.3 to +1.5 V until the voltammograms were reproducible. For preparation of Hb electrodes, solution of Hb (5 mg/mL) was prepared in 0.1 M PBS (pH 7.0) and ZHSs suspension was mixed with volume ratio of 1:1. Electro-codeposition of ZHSs entrapped of Hb was achieved by cycling the potential between −1.0 and 1.2 V at a scan rate of 150 mV s^{-1} for 30 consecutive cycles in solution containing ZHS and Hb. The modified electrode (Hb/ZHS/Au) was stored in refrigerator (4 °C) until further study.

Results and discussion

Characterization of ZHS

The TEM images of the ZHS nanoparticles were shown in Fig. 1. After calcination, the sulfonated PS core was removed completely, so perfect ZHSs were obtained. The ZHSs were in diameter of 150 nm.

In order to investigate the surface topographies of different films, AFM (Fig. 2) analysis was performed at ZHS and Hb/ZHS films modified gold substrate, respectively. As shown in Fig. 2a, the AFM micrograph of ZHS film presents clearly spherical structures, which covers the entire surface of the substrate. The AFM image (Fig. 2b) of Hb/HZS exhibits obvious differences as compared to ZHS film. Particles-like nanostructures almost disappear and the surface morphology become smoother with the appearance of stratum-like structure, which might be ascribed to Hb molecules filling the interstitial places, suggesting that the Hb were successively and effectively immobilized on ZHS film.

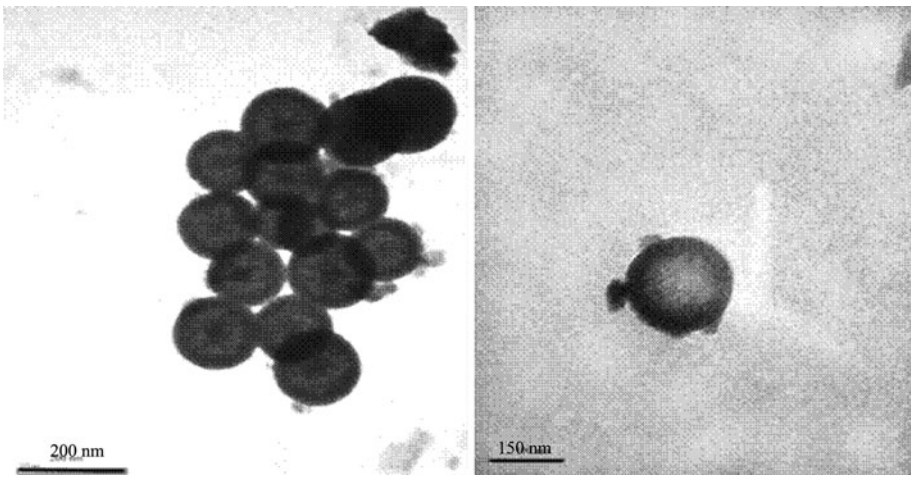

Fig. 1 TEM images of ZHS

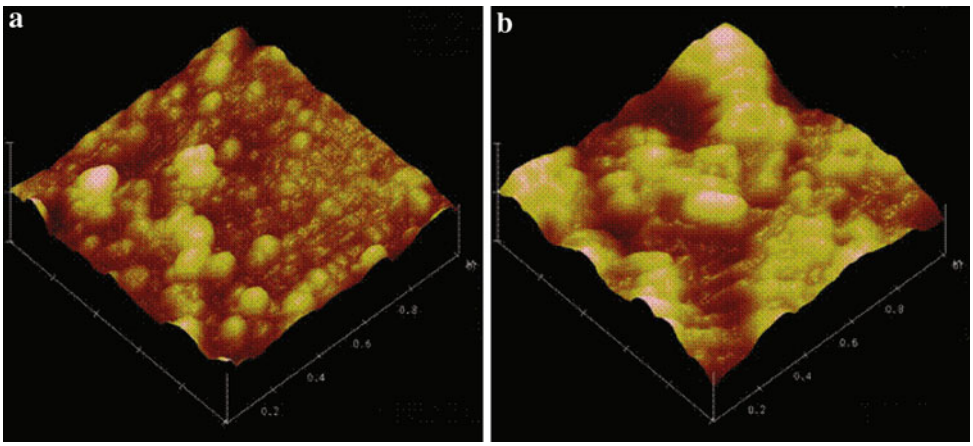

Fig. 2 AFM images of ZHS (**a**) and Hb/HZS (**b**)

UV–vis spectroscopic analysis

UV–vis spectroscopy is sensitive for the characteristic structure of proteins. Figure 3 shows the UV–vis absorption of ZHS, Hb and Hb/ZHS, respectively. From Fig. 3, the Soret absorption band of Hb entrapped in ZHS locates at about 404 nm (curve b), which is close to that of natural Hb (i.e. 407 nm, curve a), while ZHS does not show absorption bands in the wavelength range (curve c). Obviously, the absorption peak is attributed to the Soret band of Hb. This result suggests that Hb retains its biological activity.

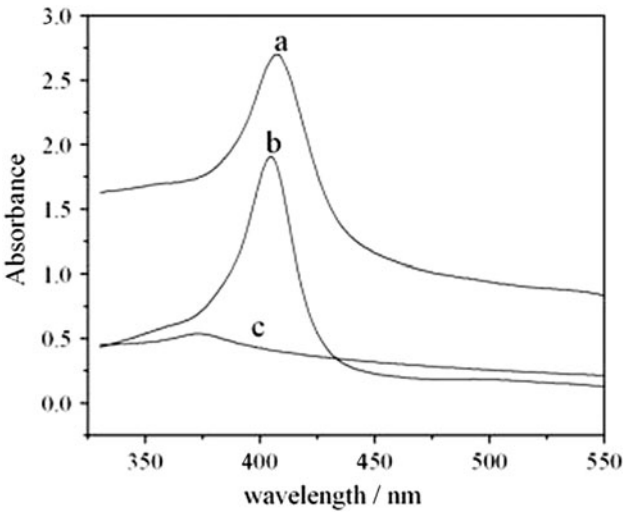

Fig. 3 UV–vis spectra of Hb in solution (**a**), Hb/ZHS (**b**), and ZHS (**c**)

Direct electrochemistry of Hb/ZHS-modified electrode

The electrochemical behavior of Hb/ZHS film modified Au electrode (Hb/ZHS/Au) was studied by cyclic voltammetry (CV). Figure 4 shows the cyclic voltammograms (CVs) of bare Au electrode, ZHS/Au and Hb/ZHS/Au in pH 7.0 PBS were recorded at 50 mV/s. There is no redox peaks for bare Au electrode (Fig. 4a) and ZHS/Au (Fig. 4b), while a couple of stable and well-defined peaks can be observed at Hb/ZHS/Au electrode (Fig. 4c). Obviously, the responses of the modified electrodes are attributed to the redox of immobilized Hb. The ZHS matrix can be favorable for Hb adsorption into ZHS and enhance enzyme-loading ability. Moreover, good biocompatibility of ZHS retains

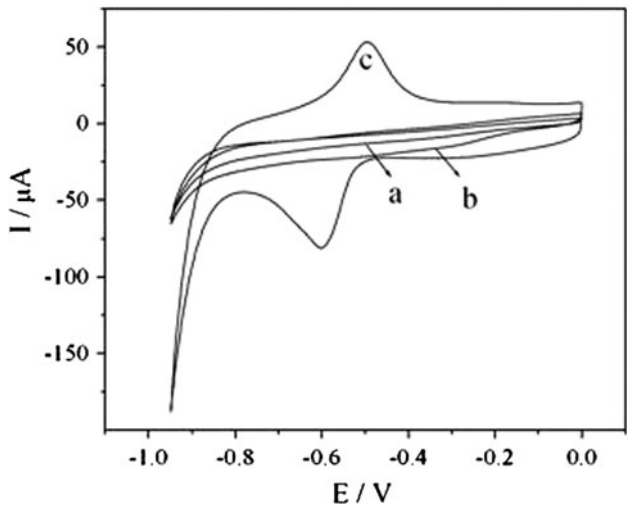

Fig. 4 CVs of bare Au electrode (**a**), ZHS/Au (**b**), and Hb/ZHS/Au (**c**) in 0.1 M PBS (pH 7.0), scan rate 50 mV/s

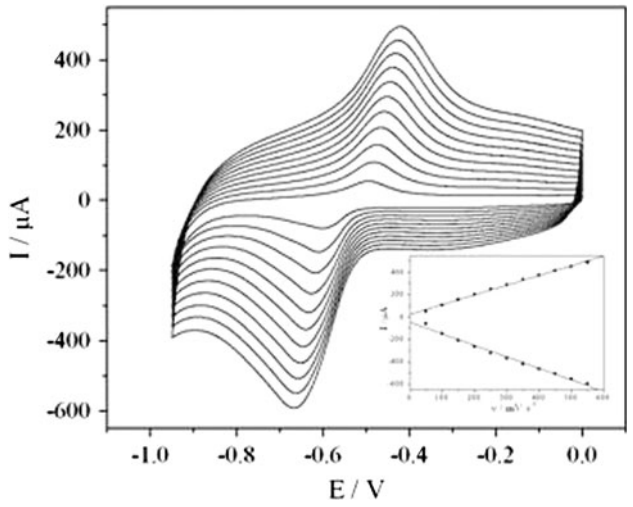

Fig. 5 Cyclic voltammograms of the biosensor at different scan rates (from inner to outer): 50, 100, 150, 200, 250, 300, 350, 400, 450, 500, 550 mV/s in 0.1 M PBS (pH 7.0). *Inset* Plot of peak currents versus scan rates

bioactivity of Hb, which is also important in realizing the direct electron transfer between Hb and Au electrode.

Figure 5 gives typical CVs of the Hb/ZHS modified electrode with scan rates from 0.05 to 0.55 V s^{-1}. With the increase of the scan rates, the cathodic and anodic peak currents of Hb increased simultaneously, as shown in the inset of Fig. 5, and the cathodic and anodic peak currents increased linearly with scan rates from 0.05 to 0.55 V s^{-1}, indicating the redox reaction is a surface process [22].

For such a surface process, the average surface coverage (Γ) can be calculated according to the Laviron equation [23],

$$I_P = \frac{n^2F^2vA\Gamma}{4RT} = \frac{nFQv}{4RT}$$

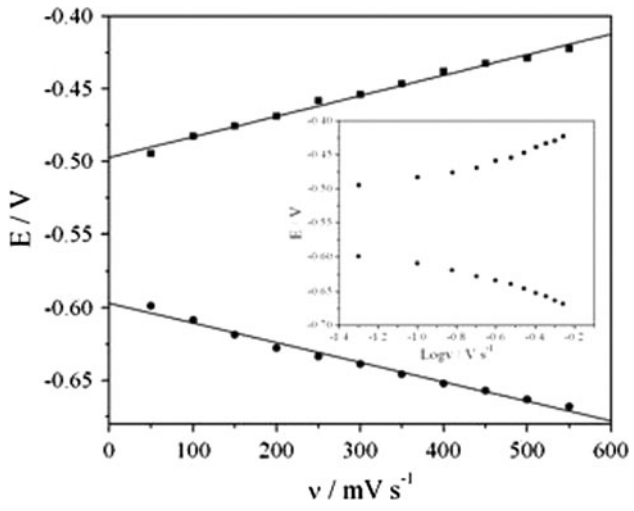

Fig. 6 Various of peak potentials versus the scan rates. *Inset* plot of ΔE_p versus log*v*

where *A* was the surface area, *n* was the number of electrons transferred, *Q* was the total amount of charge, and *F* was the Faraday constant. From the CV curves, *Q* and I_P were calculated to be 6.746×10^{-5} C and 1.421×10^{-4} A after background correction, respectively. Thus, the number of electrons transferred for the direct electron transfer reaction of Hb was calculated to be $n = 1$, suggesting that a single electron-transfer reaction occurred at the Hb/ZHS/Au, and the average surface concentration (Γ) of Hb was calculated to be 4.54×10^{-10} mol/cm^2. As the theoretical monolayer coverage for Hb is about 1.8×10^{-11} mol/cm^2 [24], it can be proposed that many layers of Hb immobilized near electrode surface undergo electrochemical reaction.

According to the Laviron theory, the transfer coefficient (α) and electron-transfer rate constant (k_s) can be estimated by measuring the variation of peak potential with scan rate (Fig. 6) [25]. From the inset of Fig. 6, the slope of the curves the further relationship of ΔE_p with logυ (V s^{-1}) was achieved. The transfer coefficient (α) and electron-transfer rate constant (k_s) were 0.5 and 3.1 s^{-1}, respectively. The value for electron-transfer rate constant was higher than electron-transfer rate constant of Hb in layered a-ZrP, 1.85 ± 0.51 s^{-1} [26], and Nafion/nano-ZnO film, 0.139 s^{-1} [27], It is assumed that the ZHSs nanoparticles increased the surface area and active point for entrapping Hb. ZHSs nanoparticles has good biocompatibility, which could retain the bioactivity of Hb and enhance the direct electron transfer of Hb.

Electrochemical response to hydrogen peroxide of the biosensor

The electrochemical behavior of Hb/ZHS film modified Au (Hb/ZHS/Au) was studied by CV. Figure 7 shows the bioelectrocatalytic behavior of the enzyme electrode in

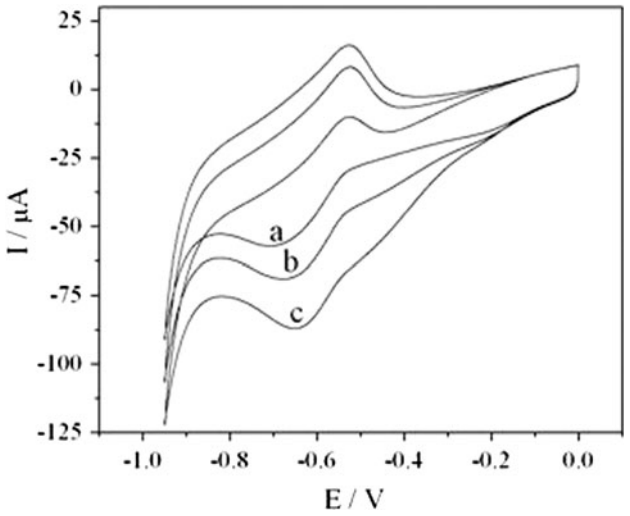

Fig. 7 Cyclic voltammograms of Hb/ZHS/Au electrode with 0 (**a**), 3.5×10^{-4} (**b**) and 7.0×10^{-4} M H_2O_2 (**c**) in 0.1 M PBS (pH 7.0), scan rate 100 mV/s

0.1 M PBS of pH 7.0. Upon addition of H_2O_2, the reduction peak current increases at about −0.65 V and the anodic peak current decreases dramatically, indicating a typical electrocatalytic reduction process of H_2O_2. The cathodic peak current increases dramatically, indicating the reduction of H_2O_2 was catalyzed by the Hb immobilized on the ZHS film and the Hb kept its natural structure.

Effect of solution pH on direct electron transfer of Hb

The direct electrochemistry of Hb immobilized on ZHS showed a strong dependence on solution pH. A pair of stable and well-defined redox peaks was obtained in different pH solution. With pH increasing from 5.0 to 8.5, the maximum peak currents of Hb occurs at pH 7.0 (Fig. 8) and

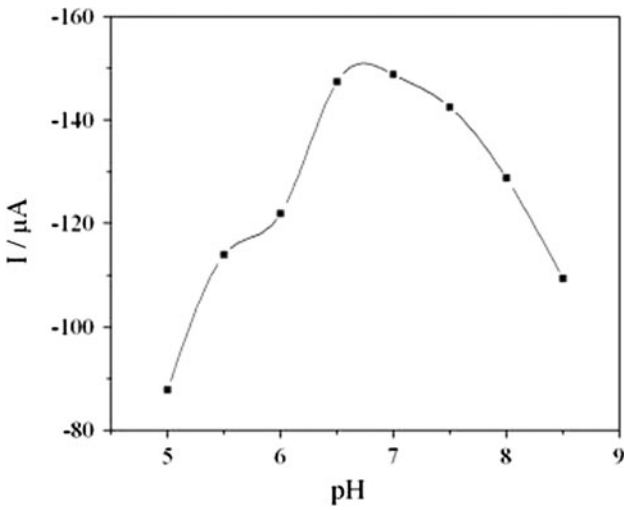

Fig. 8 Dependence of the current response of Hb/ZHS/Au electrode to 3.5×10^{-4} mol/L H_2O_2 on different pH of buffer solutions

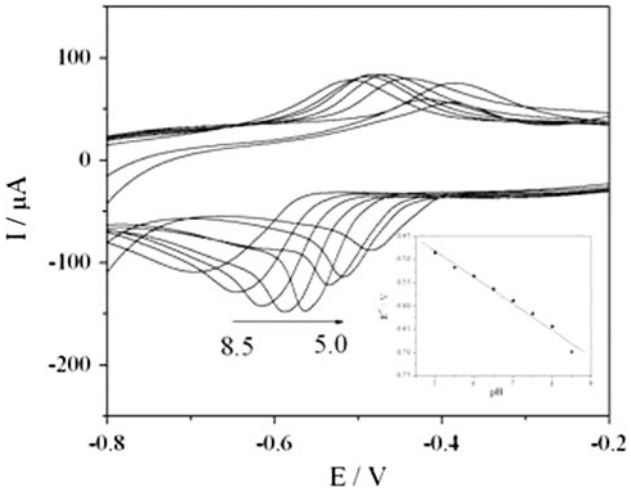

Fig. 9 Cyclic voltammograms of Hb/ZHS/Au in 0.1 M PBS at different pH, from left to right 8.5–5.0 at a scan rate of 100 mV/s. *Inset* plot of formal potential versus pH

both cathodic and anodic peaks potentials shifts negatively (Fig. 9). All changes in voltammetric peak potentials and currents with pH are reversible. The formal potential $E^{\circ\prime}$ shifts of 57 mV/pH unit between pH 5.0 and 8.5 (inset in Fig. 9), which is reasonably close to the expected value (59 mV/pH) for one electron and one proton reaction [28]. This indicated that a single proton transfer coupled to the single electron transfer in order to neutralize the excess charge on the electrochemical interface [29]. Thus, the reaction equation for the electrochemical reduction of Hb may be described as follows [30]:

$$\mathrm{HbFe(III)} + \mathrm{H^+} + \mathrm{e^-} = \mathrm{HbFe(II)}.$$

Effect of applied potential

The effect of applied potential on the steady-state current of the biosensor was shown in Fig. 10. Amperometric current increases gradually when the applied potential shifts negatively from 0.1 to −0.6 V, which might be attributed to the increased driving force for the fast reduction of Hb at low potentials. At an applied potential of −0.45 V, the relative constant current appeared, and the background current and noise level reached their lowest value, which indicates that interfering reactions of other electroactive species were minimized at the potential in PBS. Therefore, −0.45 V was chosen as working potential for the following measurements.

Electrocatalytic reduction of H_2O_2 on Hb/ZHS/Au electrode

The amperometric response of the hydrogen peroxide biosensor was investigated by successively adding H_2O_2 of

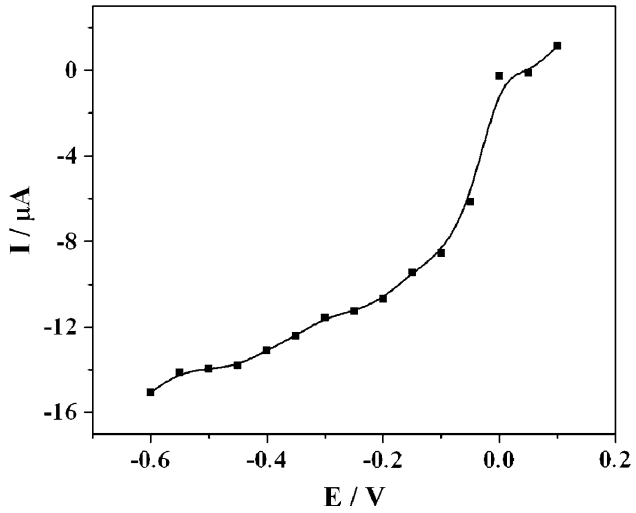

Fig. 10 Dependence of the current response on the applied potential at Hb/ZHS/Au electrode in the presence of 0.35 mM H_2O_2 in 0.1 M PBS (pH 7.0)

different concentration to a continuous stirring PBS (pH 7.0) solution. The electrocatalytic reduction peak potential (i.e. −0.45 V) was selected as the constant applied potential for the high sensitivity together with a wide linear range. Upon addition of H_2O_2 to the PBS, a stepwise growth of reduction current was observed (Fig. 11). The modified Au electrode achieved 95% of the steady current towards H_2O_2 in less than 5 s, which indicated that the electrocatalytic response was very fast. It attributes that the ZHS thin film provides a platform to enhance Hb immobilization and provides a compatible microenvironment for Hb adsorption. The inset of Fig. 11 shows the

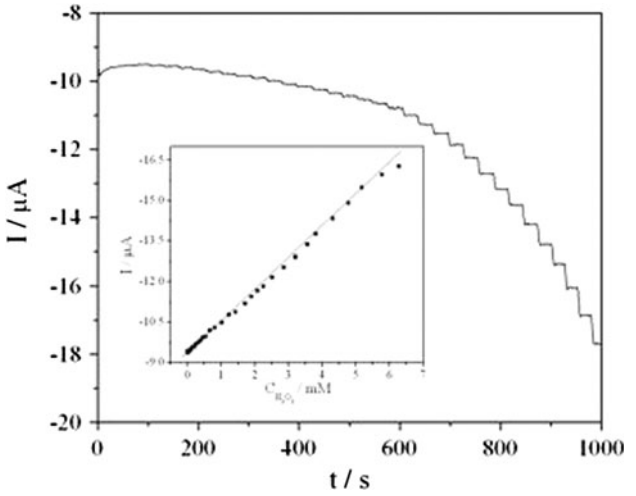

Fig. 11 Typical current–time response of the biosensor on successive injection of different concentration of H_2O_2 into a stirred solution of 0.1 M PBS (pH 7.0) at an applied potential of −0.45 V in the time intervals of 30 s. *Inset* calibration plot of currents versus H_2O_2 concentrations

amperometric current had a good linear relationship with the concentration of H_2O_2 in the range of 2.1×10^{-6} –5.18×10^{-3} M and the linear regression equation was I(μA) = −0.936 C (μM)−0.114 ($R^2 = 0.9993$, $n = 31$). From the slope of calibration curve, its detection limit is 7×10^{-7} M (S/N = 3). The performance of the present biosensor is better than other Hb biosensor, such as Hb–PCL/GC electrode (linear range 2×10^{-6}–3×10^{-5} M, detection limit 6.07×10^{-6} M [31], GNSs/APTES/ITO electrodes (linear range 5×10^{-6}–1×10^{-3} M, detection limit 3.4×10^{-6} M) [32], Hb/MCMS/GCE (linear range 6.9×10^{-5}–2.3×10^{-2} M, detection limit 2.1×10^{-5} M) [33], which is attributed to the good mass transport, larger Hb protein loading per unit area and fast electron-transfer rate of the immobilized Hb protein.

When the concentration of H_2O_2 was higher than 5.18 mM, a response plateau was observed, showing a typical Michaelis–Menten kinetic mechanism. The apparent Michaelis–Menten constant (K_M^{app}), which gives an indication of the enzyme–substrate kinetics, could be calculated from the Lineweaver–Burk equation [34]:

$$1/I_{ss} = 1/I_{max} + K_M^{app}/I_{max}C$$

where I_{ss} was the steady current, I_{max} was the current measured when H_2O_2 was saturation in PBS solution and C was the concentration of H_2O_2. The value for this H_2O_2 biosensor was calculated to be 0.5 mM from Lineweaver–Burk equation. This value is smaller than those of Hb immobilized onto ZrO_2, 1.77 mM [35], Hb immobilized onto mesoporous tungsten oxide, 1.84 mM [36], Hb immobilized onto Ti(III)–TNTs, 1.02 mM [37], suggesting a higher affinity to H_2O_2 and a higher enzymatic activity to H_2O_2 reduction for the adsorption of Hb into ZHS.

Comparison with other hydrogen peroxide biosensors-based ZnO nanocomposites

The analytical performances of the proposed biosensor were compared with other hydrogen peroxide biosensors reported in the literatures. The results were shown in Table 1. In contrast with other H_2O_2 biosensors reported so far (Table 1) [18, 38–42], Hb/ZHS/Au electrode shows the widest linear detection range and lower detection limit. These indicate that Hb/ZHS/Au electrode is an excellent platform for the detection of H_2O_2.

Selectivity and stability of the hydrogen peroxide biosensor

The selectivity of this H_2O_2 biosensor was evaluated by H_2O_2 determinations in the presence of some potentially coexisting compounds of H_2O_2 in biological systems. The degree of interference from interfering substances can be

Table 1 Analytical properties of H_2O_2 biosensors based on ZnO nanocomposites

S. No.	Material	Structure of electrode	Detection limit (μM)	Linear range (μM)	References
1	Gold nanoshells	GNSs/APTES/ITO electrodes	3.4	5–1,000	[32]
2	ZnO nanosheets	ZnO/cyt. c. electrode	0.8	1–1,000	[38]
3	Flower-like ZnO crystals	ZnO–Chitosan/Nanogold–HRP	0.7	1.5–450	[39]
4	Porous nanosheet-based	Hb–ZnO–Nafion/GC electrode ZnO microspheres		1–410	[18]
5	Flowerlike ZnO	ZnO–GNPs–Nafion-HRP/GC electrode	9.0	15–1,100	[40]
6	Fork like ZnO	Complex multiple fork like ZnO nanostructure/ CHIT/HRP electrode	0.3	50–700	[41]
7	Nanoporous ZnO	Mb-ZnO-modified GE electrode	2	4.8–200	[42]
8	Poly allylamine	PAA/Hb Au electrode	0.2	2.5–500	[43]
9	Carbon nanotubes	Polymer-Hb-DMWNTs	0.8	5–600	[44]
10	ZnO hollow spheres	Hb/ZHS/Au electrode	0.7	2.1–5,180	Present work

evaluated by the value of the current ratio which were calculated by reading the current of the proposed biosensor in an assay solution containing 0.20 mM H_2O_2 and a 0.20 mM interfering substance and comparing it with the current from the proposed biosensor in the same assay solution containing only 0.20 mM H_2O_2. In the experiment, six interfering substances were used to evaluate the selectivity of the biosensor. The results are listed in Table 2. It can be observed that the six tested interferences exerted negligible influences on the determination of H_2O_2. So, it is showing the proposed biosensor possesses a good selectivity, which is attributed to the good biocompatibility of the ZHS.

The storage stability of the proposed biosensor was also studied. The biosensor was immersed in 0.1 M PBS (pH 7.0) at 4 °C when not used. The biosensor decreased 3.5, 8.8, and 16.3% of the initial response after 5 days, 2 weeks, and 1 month storage, respectively. The good storage stability was ascribed to the good biocompatibility of the ZHS biocomposite.

Table 2 Possible interferences tested with the hydrogen peroxide biosensor

Possible interferences	Current ratio
L-Cysteine	0.98
L-Tyrosine	0.96
Ethanol	0.97
Glucose	1.03
Acetic acid	1.00
Ascorbic acid	1.02

Ratio of currents for mixtures containing 0.2 mM interfering substance and 0.2 mM H_2O_2 to that for 0.2 mM H_2O_2 alone

Conclusions

In this work, the Hb and biocompatible composite ZHS were successfully electro-codeposited onto the surface of gold electrode. When Hb was immobilized on Au surface by the ZHS, a quasi-reversible CV response for Hb Fe(III)/Fe(II) was obtained. The good performance of Hb/ZHS/Au electrode indicates these nanoparticles provided a suitable matrix for protein immobilization and well-kept the bioactivities of protein. Such ZHS was found to possess better direct electron-transfer properties, and good biocompatibility. The prepared third-generation biosensor displayed good sensitivity and reproducibility, wide linear range, low detection limit, fast response and good long-term stability for the detection of H_2O_2. The ZHS can provide a good electrochemical sensing platform for the applications in biosensor and biocatalysis.

References

1. Armstrong FA (2002) Insights from protein film voltammetry into mechanisms of complex biological electron-transfer reactions. J Chem Soc Dalton Trans 5:661–671
2. Willner I, Katz E (2000) Integration of layered redox-proteins and conductive supports for bioelectronic applications. Angew Chem Int Ed 39:1180–1218
3. Hill HAO (1996) The development of bioelectrochemistry. Coord Chem Rev 151:115–123
4. Yu JJ, Zhao T, Zhao FQ et al (2008) Direct electron transfer of hemoglobin immobilized in a mesocellular siliceous foams supported room temperature ionic liquid matrix and the electrocatalytic reduction of H_2O_2. Electrochim Acta 53:5760–5765
5. He XY, Zhu L (2006) Direct electrochemistry of hemoglobin in cetylpyridinium bromide film: redox thermodynamics and electrocatalysis to nitric oxide. Electrochem Commun 8:615–620
6. Lu Q, Zhou T, Hu SS (2007) Direct electrochemistry of hemoglobin in PHEA and its catalysis to H_2O_2. Biosens Bioelectron 22:899–904
7. He PL, Hu NF, Rusling JF (2004) Driving Forces for layer-by-layer self-assembly of films of SiO_2 nanoparticles and heme proteins. Langmuir 20:722–729

8. Xian YZ, Xian Y, Zhou LH et al (2007) Encapsulation hemoglobin in ordered mesoporous silicas: Influence factors for immobilization and bioelectrochemistry. Electrochem Commun 9:142–148
9. Bistolas N, Wollenberger U, Jung C et al (2005) Cytochrome P450 biosensors—a review. Biosens Bioelectron 20:2408–2423
10. Huang H, Hu NF, Zeng Y et al (2002) Electrochemistry and electrocatalysis with heme proteins in chitosan biopolymer films. Anal Biochem 308:141–151
11. Lu XB, Wen ZH, Li JH (2006) Hydroxyl-containing antimony oxide bromide nanorods combined with chitosan for biosensors. Biomaterials 27:5740–5747
12. Chen D, Liu JS, Wang P et al (2007) Fabrication of monodisperse zirconia-coated core–shell and hollow spheres in mixed solvents. Colloids Surf A: Physicochem Eng Aspects 302:461–466
13. Graf C, Blaaderen AV (2002) Metallodielectric colloidal core–shell particles for photonic applications. Langmuir 18:524–534
14. Liu RJ, Li YJ, Zhao H et al (2008) Synthesis and characterization of Al_2O_3 hollow spheres. Mater Lett 62:2593–2595
15. Kalele SA, Ashtaputre SS, Hebalkar NY et al (2005) Optical detection of antibody using silica–silver core–shell particles. Chem Phys Lett 404:136–141
16. Applerot G, Lipovsky A, Dror R et al (2009) Enhanced antibacterial activity of nanocrystalline ZnO due to increased ROS-mediated cell injury. Adv Funct Mater 19:842–852
17. Liu ZM, Liu YL, Yang HF et al (2005) A mediator-free tyrosinase biosensor based on ZnO sol–gel matrix. Electroanalysis 17:1065–1070
18. Lu XB, Zhang HJ, Ni YW et al (2008) Porous nanosheet-based ZnO microspheres for the construction of direct electrochemical biosensors. Biosens Bioelectron 24:93–98
19. Li XF, Lv KL, Deng KJ et al (2009) Synthesis and characterization of ZnO and TiO_2 hollow spheres with enhanced photoreactivity. Mater Sci Eng B 158:40–47
20. Agrawal M, Gupta S, Pich A et al (2009) A facile approach to fabrication of ZnO–TiO_2 hollow spheres. Chem Mater 21:5343–5348
21. Deng ZW, Chen M, Gu GX et al (2008) A facile method to fabricate ZnO hollow spheres and their photocatalytic property. J Phys Chem B 11:216–222
22. Murray RW, Bard AJ (1984) Electroanalytical chemistry, vol 13. Marcel Dekker, New York, pp 191–368
23. Laviron E (1974) Adsorption autoinhibition and autocatalysis in polarography and in linear potential sweep voltammetry. J Electroanal Chem 52:355–393
24. Liu HH, Tian ZQ, Lu ZX et al (2004) Direct electrochemistry and electrocatalysis of heme-proteins entrapped in agarose hydrogel films. Biosens Bioelectron 20:294–304
25. Laviron E (1979) The use of linear potential sweep voltammetry and of a.c. voltammetry for the study of the surface electrochemical reaction of strongly adsorbed systems and of redox modified electrodes. J Electroanal Chem 100:263–270
26. Liu YG, Lu CL, Hou WH et al (2008) Direct electron transfer of hemoglobin in layered a-zirconium phosphate with a high thermal stability. Anal Biochem 375:27–34
27. Sun W, Zhai ZQ, Wang DD et al (2009) Electrochemistry of hemoglobin entrapped in a Nafion/nano-ZnO film on carbon ionic liquid electrode. Bioelectrochemistry 74:295–300
28. Nassar AE, Zhang Z, Hu N et al (1997) Proton coupled electron transfer from electrodes to myoglobin in ordered biomembrane-like films. J Phys Chem B 101:2224–2231
29. Huang H, He P, Hu N et al (2003) Electrochemical and electrocatalytic properties of myoglobin and hemoglobin incorporated in carboxymethyl cellulose films. Bioelectrochemistry 61:29–38
30. Trushina E, Oda R, Landers J et al (1997) Determination of nitrite and nitrate reduction by capillary ion electrophoresis. Electrophoresis 18:1890–1898
31. Zheng W, Li J, Zheng YF (2008) An amperometric biosensor based on hemoglobin immobilized in poly(ε-caprolactone) film and its application. Biosens Bioelectron 23:1562–1566
32. Wang Y, Qian WQ, Tan Y et al (2007) Direct electrochemistry and electroanalysis of hemoglobin adsorbed in self-assembled films of gold nanoshells. Talanta 72:1134–1140
33. Lai GS, Zhang HL, Han DY (2008) A novel hydrogen peroxide biosensor based on hemoglobin immobilized on magnetic chitosan microspheres modified electrode. Sensors Actuators B 129: 497–503
34. Kamin A, Wilson GS (1980) Rotating ringdisk enzyme electrode for biocatalysis kinetic studies and characterization of the immobilized enzyme layer. Anal Chem 52:1198–1205
35. Zhao G, Feng JJ, Xu J et al (2005) Direct electrochemistry and electrocatalysis of heme proteins immobilized on self assembled ZrO_2 film. Electrochem Commun 7:724–729
36. Feng JJ, Xu JJ, Chen HY (2005) Direct electron transfer and electrocatalysis of hemoglobin adsorbed onto electrodeposited mesoporous tungsten oxide. Electrochem Commun 8:77–82
37. Liu MC, Zhao GH, Zhao KJ et al (2009) Direct electrochemistry of hemoglobin at vertically aligned self-doping TiO_2 nanotubes: a mediator-free and biomolecule-substantive electrochemical interface. Electrochem Commun 11:1397–1400
38. Rui Q, Komori KK, Tian Y et al (2010) Electrochemical biosensor for the detection of H_2O_2 from living cancer cells based on ZnO nanosheets. Anal Chim Acta 670:57–62
39. Zhang YW, Zhang Y, Wang H et al (2009) An enzyme immobilization platform for biosensor designs of direct electrochemistry using flower-like ZnO crystals and nano-sized gold particles. J Electroanal Chem 627:9–14
40. Xiang CL, Zou YJ, Sun LX et al (2009) Direct electrochemistry and enhanced electrocatalysis of horseradish peroxidase based on flowerlike ZnO–gold nanoparticle—Nafion nanocomposite. Sens Actuators B 136:158–162
41. Yang Z, Zong XL, Ye ZZ et al (2010) The application of complex multiple fork like ZnO nanostructures to rapid and ultrahigh sensitive hydrogen peroxide biosensors. Biomaterials 31:7534–7541
42. Zhao G, Xu JJ, Chen H (2006) Interfacing myoglobin to graphite electrode with an electrodeposited nanoporous ZnO film. Anal Biochem 350:145–150
43. Kafi AKM, Lee DY, Park SH et al (2007) Amperometric biosensor based on direct electrochemistry of hemoglobin in poly allylamine (PAA) film. Thin Solid Films 515:5179–5183
44. Chen L, Lu GX (2007) Novel amperometric biosensor based on composite film assembled by polyelectrolyte-surfactant polymer, carbon nanotubes and hemoglobin. Sens. Actuators B 121:423–429